Commun Nonlinear Sci Numer Simulat 14 (2009) 4176–4190

Contents lists available at ScienceDirect

Commun Nonlinear Sci Numer Simulat

journal homepage: www.elsevier.com/locate/cnsns

Local expansion concepts for detecting transport barriers in dynamical systems

Kathrin Padberg [a,b], Bianca Thiere [c,*], Robert Preis [c], Michael Dellnitz [c]

[a] Institute for Transport and Economics, Technische Universität Dresden, D-01062 Dresden, Germany
[b] Center for Information Services and High Performance Computing, Technische Universität Dresden, D-01062 Dresden, Germany
[c] Faculty of Computer Science, Electrical Engineering and Mathematics, University of Paderborn, D-33095 Paderborn, Germany

ARTICLE INFO

Article history:
Received 16 October 2008
Received in revised form 19 March 2009
Accepted 19 March 2009
Available online 27 March 2009

PACS:
05.10.−a
05.60.Cd
02.60.−x
05.45.−a

Keywords:
Transport barriers
Dynamical systems
Almost invariant sets
Graph theory
Set-oriented methods
Expansion
Invariant manifolds

ABSTRACT

In the last two decades, the mathematical analysis of material transport has received considerable interest in many scientific fields such as ocean dynamics and astrodynamics. In this contribution we focus on the numerical detection and approximation of transport barriers in dynamical systems. Starting from a set-oriented approximation of the dynamics we combine discrete concepts from graph theory with established geometric ideas from dynamical systems theory. We derive the global transport barriers by computing the local expansion properties of the system. For the demonstration of our results we consider two different systems. First we explore a simple flow map inspired by the dynamics of the global ocean. The second example is the planar circular restricted three body problem with Sun and Jupiter as primaries, which allows us to analyze particle transport in the solar system.

1. Introduction

The transport of material constitutes an important aspect of many natural systems. During the last two decades different mathematical concepts have been developed to get a better understanding of the mechanisms of particle transport and to estimate transport rates and probabilities, in particular in the context of Hamiltonian systems, see e.g. [1–7] and references therein as well as [8] for a recent review on perturbation theory. Areas of application cover many scientific fields, such as fluid dynamics, ocean dynamics, molecular dynamics, physical chemistry, and astrodynamics (e.g. [7,9–11]).

The mathematical analysis of transport phenomena is characterized by a high complexity. Generally, the approximation of barriers to transport is only possible by numerical methods, often even involving heuristic concepts. The different approaches fall roughly into two classes, geometric and probabilistic concepts, see [12] for a recent discussion and comparison.

An established geometrical approach for the analysis of transport phenomena relies on the approximation of stable and unstable manifolds of hyperbolic objects such as fixed points, periodic orbits, or, possibly, cantori. Their transversal intersection gives rise to complicated dynamical behavior and explains transport in terms of lobe dynamics [3,1], i.e.

* Corresponding author. Tel.: +49 5251 60 2656; fax: +49 5251 60 4216.
E-mail address: thiere@math.upb.de (B. Thiere).

1007-5704/$ - see front matter © 2009 Elsevier B.V. All rights reserved.
doi:10.1016/j.cnsns.2009.03.018

transport over the manifold-related boundaries can be quantified by estimating enclosed volumes in the homoclinic or heteroclinic tangle.

In this context finite-time Lyapunov exponents (FTLE) [4,13–15,6] are increasingly used (especially in nonautonomous systems) for the approximation of transport barriers and invariant manifolds. This quantity measures how much a small initial perturbation evolves under the (linearized) dynamics and it is expected to be large in the vicinity of invariant manifolds of hyperbolic objects. This way, local maxima or ridges in the scalar FTLE field typically define boundaries between regions that are characterized by a minimal exchange of particles [6].

From a probabilistic point of view *almost invariant sets* of a dynamical system are an important characteristic for analyzing questions related to transport. An almost invariant set is a subset of state space where typical trajectories stay for a long period of time before they enter other parts of the state space. It is important to find out the number as well as the positions of the almost invariant sets, i.e. regions that do not communicate freely with each other in terms of particle transport.

Based on a set-oriented approach the solution to this problem can be reduced to analyzing a finite-state Markov process, see e.g. [16–21]. In this setting the dynamics is approximated by a transition matrix. Its entries are the transition probabilities between small compact disjunct sets (boxes), which form a set-oriented discretization of the region of interest (e.g. a covering of the global attractor of the dynamical system). Note that the transition matrix is a finite approximation of the respective transfer (or Frobenius–Perron) operator that describes the evolution of densities or measures. Its spectral properties provide useful means for the approximation of almost invariant sets and thus for barriers to particle transport.

The discretized dynamical system induces a weighted directed graph in a very natural way, with vertices corresponding to boxes and edges to non-zero entries in the transition matrix. The search for almost invariant sets in the dynamical system can now be translated into finding vertex partitions in the graph which exhibit a small number (or sum of weights) of cutted edges, i.e. of edges connecting the different sets (see e.g. [20,22,7]). For this task we can rely on graph partitioning algorithms as there has been a high research activity in this field to solve problems from several applications like e.g. the efficient use of parallel and distributed computers, VLSI-design, data mining and many others. Although most graph partitioning problems are **NP**-complete, there are a number of theoretical upper and lower bounds, as well as many heuristics of different background. Furthermore, several software tools for graph partitioning are available.

Set-oriented numerical methods in combination with graph algorithmic techniques have thus been successfully applied for the identification of the number and location of almost invariant sets in state space [20,22,7]. The concept of almost invariant sets provides a partition of phase space that does not explicitly use the geometrical template of invariant manifolds. The focus of the almost invariant sets is the separation of the center regions of each set with the boundaries between them as a by-product. Furthermore, the almost invariant sets do not provide us with information about the quality of the boundaries such as a quantification of how strongly they repel particles. This is a motivation for us to look at other characteristics of transport barriers in order to get this additional information.

Typically the boundaries between the almost invariant sets coincide with invariant manifolds of hyperbolic periodic points as demonstrated in [7,12]. Our new idea is therefore to approximate these manifolds by calculating local expansion properties, i.e. we exploit that the system typically has a high expansion close to a barrier and a low expansion further away from a barrier. The values of the expansion then give us information about quality or strength of the barriers. There exist different basic concepts of expansion properties in dynamical systems theory as well as in graph theory. However, here we will use them in the set-oriented setting in order to compute the invariant manifolds and, thus, the transport barriers.

In order to exhibit the local expansion we consider and combine several techniques for the mathematical treatment of transport processes – using both continuous concepts from dynamical systems theory (e.g. invariant manifolds, finite-time Lyapunov exponents) and discrete ideas from graph theory (e.g. local subgraph expansion values). The resulting techniques are an extension of the ideas described in [7,23,24].

The paper is organized as follows: first we present a short mathematical description of transport and the related concept of almost invariant sets. Section 3 contains a brief overview of the set-oriented approach which forms the basis for our concepts. The notion of almost invariant sets can be transformed into the set-oriented setting and further translated into a graph formulation. Thus, we are able to apply graph partitioning techniques for the approximation of almost invariant sets. Section 4 is devoted to the local expansion concepts for the detection of invariant manifolds and transport barriers. We first describe the expansion rate based on the finite-time Lyapunov exponent approach. We then continue with the description of the graph based local expansion rate. It is calculated for each vertex in the graph by using the expansion property of a local neighborhood of the vertex. Finally, we exploit the multilevel structure of the underlying set-oriented ansatz for the development of adaptive techniques. These allow us to obtain a high numerical accuracy while keeping the computational costs acceptable. After having presented the theory and numerical background of our approach we demonstrate the application of our results in Sections 5 and 6. In Section 5 we consider a Poincaré map in the Double Gyre Flow [6], a simple periodically forced system inspired by the dynamics of the global ocean. In Section 6 we analyze transport in the solar system by means of a first return map in the Planar Circular Restricted Three Body Problem (PCRTBP) with the Sun and Jupiter as the primaries. We conclude with a discussion of our results and of future research directions.

2. Transport and almost invariant sets

A continuous map $f : M \to M$ on a compact subset $M \subset \mathbb{R}^n$ defines a discrete dynamical system

$$x_{k+1} = f(x_k), \quad k = 0, 1, \ldots$$

Often this system is given in terms of a time-T map or a Poincaré return map of some ordinary differential equation. Then f is even a diffeomorphism, which we assume to be the case in the remainder of this contribution.

Generally, the analysis of particle transport is a question about the macroscopic dynamics of f. One is interested in the evolution of sets or, more precisely, densities or measures on M rather than in single trajectories. The evolution of measures v on M can be described in terms of the transfer operator (or Perron–Frobenius operator) associated with f. This is a linear operator $P : \mathscr{M} \to \mathscr{M}$,

$$(Pv)(A) = v(f^{-1}(A)), \quad A \text{ measurable}, \tag{1}$$

on the space $\mathscr{M}$ of signed measures on M.

An invariant measure μ is a probability measure that satisfies

$$\mu(A) = \mu(f^{-1}(A)) = (P\mu)(A) \quad \text{for all measurable } A \subset M,$$

and thus is a fixed point of the transfer operator. In the following we assume that f is area and orientation preserving. Then the natural invariant measure for f is the (normalized) Lebesgue measure.

For any two sets $A_i, A_j \subset M$ with $A_i \cap A_j = \emptyset$ we can define the transition (or transport) probability ρ from A_i to A_j as

$$\rho(A_i, A_j) := \frac{m(A_i \cap f^{-1}(A_j))}{m(A_i)},$$

whenever $m(A_i) \neq 0$, where m denotes Lebesgue measure. The transition probability $\rho(A) := \rho(A, A)$ from a set $A \subset M$ to itself is called the invariance ratio of A. A set is called *almost invariant* if this quantity is very close to one [16]. For the analysis of transport phenomena it is of interest to separate the compact subset M into several disjoint subsets such that each of them is close to invariance. A reasonable measure for a good separation is the average invariance ratio of all subsets being close to one, or, in other words, one seeks to maximize this quantity (denoted by "$\to$ max"). Formally the problem can be stated as follows (cf. [20]):

Problem 1 (*Almost invariant sets: continuous notion*). For some fixed $p \in \mathbb{N}^+$ find a collection of pairwise disjoint sets $\mathscr{A} = \{A_1, \ldots, A_p\}$ with $\bigcup_{1 \leqslant l \leqslant p} A_l = M$ and $m(A_l) > 0$, $1 \leqslant l \leqslant p$, such that

$$\rho(\mathscr{A}) := \frac{1}{p} \sum_{l=1}^{p} \rho(A_l) \to \max.$$

However this set-valued optimization problem is very complex and can only be solved using heuristic approaches. In the following section we describe a set-oriented approximation of the transfer operator. This forms the background for a graph partitioning problem defined in Section 3.3, whose solution is an approximate solution to Problem 1.

3. Set-oriented methods for transport analysis

3.1. Discretization of the domain $\boldsymbol{M}$

To be able to numerically deal with the continuous phase space as well as subsets of M we need a reasonable discretization of our domain.

The subdivision algorithm [25] is the core of the set-oriented approach. Starting from an initial compact set $\mathscr{B}_0 := B_0 \supset M$ it generates a sequence $\mathscr{B}_1, \mathscr{B}_2, \ldots$ of finite collections of compact subsets (boxes) of $\mathbb{R}^n$ such that for all $k \in \mathbb{N}$,

$$Q_k = \bigcup_{B \in \mathscr{B}_k} B, \quad \text{with } B \cap B' = \emptyset \quad \text{for } B \neq B' \in \mathscr{B}_k$$

is a covering of our set of interest M (e.g. relative global attractor, recurrent set, invariant set). Moreover, the diameter of the boxes

$$\operatorname{diam}(\mathscr{B}_k) = \max_{B \in \mathscr{B}_k} \operatorname{diam}(B)$$

converges to zero as $k \to \infty$. The algorithm works in two steps, the subdivision (typically bisection in alternate coordinate directions) and a selection step, see [25,26] for details.

3.2. Approximation of the transfer operator and almost invariant sets

Let $B_i \in \mathscr{B}_k$, $i = 1, \ldots, n$, denote the boxes in the covering obtained after k steps in the subdivision algorithm. Following Ulam [27], the most natural discretization of the transfer operator P is given by the stochastic matrix $P_{\mathscr{B}} = (p_{ij})$, where

$$p_{ij} = \frac{m(f^{-1}(B_i) \cap B_j)}{m(B_j)}, \quad i,j = 1,\ldots,n, \tag{2}$$

and m denotes Lebesgue measure. So the matrix entry p_{ij} gives the probability of being mapped from box B_j to B_i in one iterate. Note that $P_{\mathscr{B}}$ is a weighted, column stochastic matrix that is typically sparse and thus defines a finite Markov chain.

With the boxes B_i being generalized rectangles, the denominator poses no problem. For the computation of $m(f^{-1}(B_i) \cap B_j)$, that is, the measure of the subset of B_j that is mapped into B_i, one can use a Monte Carlo approach as described in [28]:

$$m(f^{-1}(B_i) \cap B_j) \approx \frac{1}{K} \sum_{k=1}^{K} \chi_{B_i}(f(x_k)),$$

where the x_k's are selected at random in B_j from a uniform distribution and χ_B denotes the indicator function on B. Evaluation of $\chi_{B_i}(f(x_k))$ only means that we have to check whether or not the point $f(x_k)$ is contained in B_i. There are efficient ways to perform this check based on a hierarchical construction and storage of the collection $\mathscr{B}$ (see [25]). Note that instead of choosing an ensemble of uniformly distributed test points, we usually take points from a regular grid in order to obtain a good discretization of the respective box. This approach is particularly useful in low dimension.

The computation of $P_{\mathscr{B}}$ is fast because rather than considering the long term dynamics only one iterate of f per test point is needed. An approximation of the natural invariant measure is then given as the eigenvector of $P_{\mathscr{B}}$ corresponding to the eigenvalue 1 and will be denoted by μ. In the set-oriented setting the problem of finding almost invariant sets can now be stated as follows:

Problem 2 (*Almost invariant sets: box notation*). For some fixed $p \in \mathbb{N}^+$ find a collection of pairwise disjoint sets $\mathscr{S} = \{S_1,\ldots,S_p\}$ with $\bigcup_{1\leqslant l\leqslant p} S_l = \mathscr{B}$ and $\mu(S_l) > 0$, $1 \leqslant l \leqslant p$, such that

$$\rho(\mathscr{S}) = \frac{1}{p}\sum_{l=1}^{p} \rho(S_l) = \frac{1}{p}\sum_{l=1}^{p} \frac{\sum_{B_i,B_j\subset S_l} p_{ij}\cdot\mu(B_j)}{\sum_{B_j\subset S_l}\mu(B_j)} \to \max.$$

Although discrete, this is still a complex optimization problem. However, the sign structure of the leading eigenvectors of the transition matrix (with respect to eigenvalues very close to one) contains information about the number and location of almost invariant sets. On this spectral basis different algorithms have been derived to find good approximations to optimal partitions with respect to Problem 2 (see e.g. [16,20,29,12]).

We note that the set-oriented algorithms are implemented in the software package GAIO [26], which provides a very efficient data structure for the set-oriented discretization.

3.3. Graph formulation

The optimization problem 2 can be translated into the question of finding a specific edge-cut in a graph.

Let $G = (V,E)$ be a graph with vertex set $V = \mathscr{B}$ and directed edge set

$$E = E(\mathscr{B}) = \{(B_1,B_2) \in \mathscr{B}\times\mathscr{B} : f(B_1)\cap B_2 \neq \emptyset\}. \tag{3}$$

The function $vw : V \to \mathbb{R}$ with $vw(B_i) = \mu(B_i)$ assigns a weight to the vertices and the function $ew : E \to \mathbb{R}$ with $ew((B_i,B_j)) = \mu(B_i)p_{ji}$ assigns a weight to the edges. Furthermore, let

$$\overline{E} = \overline{E}(\mathscr{B}) = \{\{B_1,B_2\} \subset \mathscr{B} : (f(B_1)\cap B_2)\cup(f(B_2)\cap B_1) \neq \emptyset\} \tag{4}$$

be a set of undirected edges. This defines an undirected graph $\overline{G} = (V,\overline{E})$ with a weight function $\overline{ew} : \overline{E} \to \mathbb{R}$ with $\overline{ew}(\{B_i,B_j\}) = \mu(B_j)p_{ij} + \mu(B_i)p_{ji}$ on the edges. The difference between the graphs G and $\overline{G}$ is that in $\overline{G}$ the edge weight between two vertices is the sum of the edge weights of the two directed edges between the same vertices in G. Thus, the sum of all edge weights of both graphs are identical.

For a set $S \subset V$ we denote

$$C_{int}(S) = \frac{\sum_{(v,w)\in E;\, v,w\in S} ew((v,w))}{\sum_{v\in S} vw(v)} = \frac{\sum_{\{v,w\}\in\overline{E};\, v,w\in S} \overline{ew}(\{v,w\})}{\sum_{v\in S} vw(v)}$$

as the *internal cost of S*. Note that the internal cost is independent of the choice between the directed graph G or the undirected graph $\overline{G}$. Thus, we are allowed to operate on undirected graphs and we will do that in the following.

Clearly (with $V = \mathscr{B}$) a partition of $\mathscr{B}$ corresponds to a partition of V and vice versa. For a partition $\mathscr{S} = \{S_1,\ldots,S_p\}$ we denote

$$C_{int}(\mathscr{S}) = \frac{1}{p}\sum_{i=1}^{p} C_{int}(S_i) \tag{5}$$

as the *internal cost of* $\mathscr{S}$. It is an easy task to check that $\rho(\mathscr{S}) = C_{int}(\mathscr{S})$. Thus, solving Problem 2 is identical to the optimization of the internal costs of the partition $\mathscr{S}$ in Eq. (5) written in graph notation. Therefore, we have established the following graph partitioning problem.

Problem 3 (*Almost invariant sets: graph notation*). For some fixed $p \in \mathbb{N}^+$ find a collection of pairwise disjoint sets $\mathscr{S} = \{S_1, \ldots, S_p\}$ with $\bigcup_{1 \leqslant i \leqslant p} S_i = V$ and $vw(S_i) > 0$, $1 \leqslant i \leqslant p$, such that

$$C_{int}(\mathscr{S}) \to \max. \tag{6}$$

The optimization problem 3 is known to be **NP**-complete (even for constant weights, see [30]), i.e. an efficient algorithm for solving this problem is not known. It is left to say that the graph partitioning problem is **NP**-complete for most commonly used cost functions.

However, efficient graph partitioning heuristics have been developed for a number of different applications, see e.g. [31]. There are several software libraries, each of which provides a range of different methods. Examples are CHACO [32], JOSTLE [33], METIS [34], SCOTCH [35] or PARTY [31,36]. These libraries are originally designed to create solutions to the balanced partitioning problem in which all parts are restricted to have an equal (or almost equal) volume of the underlying measure. Therefore, we use parts of the library PARTY and extend them with some new code which is specially designed to address our cost function of Problem 3. More precisely, we use the tool GADS (*Graph Algorithms for Dynamical Systems*) [37,38], which efficiently interlocks the set-oriented methods of the software tool GAIO [26] with the graph partitioning library PARTY [31,36].

4. Local expansion concepts

Recent work demonstrates that almost invariant sets are typically bounded by invariant manifolds of hyperbolic objects [7,12]. We therefore briefly review the concept of expansion rates (finite-time Lyapunov exponents) for the approximation of these structures within the set-oriented approach. Further on we describe the concept of local expansion in a graph based setting.

4.1. Expansion rates based on finite-time Lyapunov exponents

We briefly review a method for the approximation of invariant manifolds of hyperbolic objects that is based on the concept of expansion rates (i.e. finite-time Lyapunov exponents). This quantity measures the maximum relative exponential divergence of small perturbations in the initial conditions over a finite time horizon. Its value is expected to be high in the vicinity of hyperbolic periodic points and their stable manifolds. This is due to the fact that two points straddling the stable manifold will experience exponential separation when approaching the hyperbolic point; likewise for the unstable manifold, when the system is considered under time-reversal, see [24] for a detailed discussion. We note that this observation is the basis for the finite-time Lyapunov approaches (e.g. [4,6]). Expansion rates for given initial condition $x_0 \in \mathbb{R}^n$ and number of iterations N are thus defined as

$$\Lambda(N, x_0) = \frac{1}{N} \log \left| \prod_{n=0}^{N-1} Df(x_n) \right|, \quad N \in \mathbb{N},$$

where $|\cdot|$ denotes the spectral matrix norm (the Euclidean vector norm, respectively).

Often the derivative $Df(x)$ is not given analytically (e.g. when f is given in terms of a Poincaré return map as in the examples we will consider). Therefore it is desirable to get an approximation of $\Lambda(N, x)$ solely on the basis of f. Let $\varepsilon > 0$ and $N \in \mathbb{N}$. The direct expansion rate is given by

$$\Lambda_\varepsilon(N, x_0) := \frac{1}{N} \log \left(\max_{\{x : |x_0 - x| = \varepsilon\}} \frac{|f^N(x_0) - f^N(x)|}{\varepsilon} \right).$$

Note that $\Lambda_\varepsilon(N, \cdot)$ is not necessarily continuous but for small ε it is a good approximation to the continuous function $\Lambda(N, \cdot)$ [24]. Here we compute a set-oriented approximation of the scalar expansion rate field. Given a box collection $\mathscr{B}_k$ that is a covering of our region of interest we define the expansion rate for a box $B \in \mathscr{B}_k$ as

$$\delta(N, B) := \max_{x_0 \in B} \Lambda(N, x_0)$$

and in an analogous way the direct expansion rate for B as

$$\delta_\varepsilon(N, B) := \max_{x_0 \in B} \Lambda_\varepsilon(N, x_0).$$

These quantities can be obtained by using an ensemble of test points in each box and taking the maximum expansion with respect to this finite set of points. For a detailed treatment of the set-oriented expansion rate approach we refer to [24].

4.2. Expansion rates based on subgraphs properties

Solutions to the graph partitioning problem as described in Section 3.3 give us some insight about the transport barriers. Graph partitioning focuses on calculating the important almost invariant sets whereas the positions of the boundaries between the parts come as a by-product. In contrast to this we would rather like to have more insight to the boundaries themselves and, thus, to get more information about the transport barriers. In order to find the transport barriers in terms of invariant manifolds we explore the use of graph-expansion values, which is a well known notion in graph theory. As the graph partitioning algorithms find almost invariant decompositions without any geometric information we also restrict ourselves to the analysis of graphs as defined above.

Graph expansion, roughly speaking, measures how much a set of vertices expands or connects to the rest of the graph. As a dynamical system has a high expansion close to an invariant manifold, the underlying graph should also have a high expansion close to the invariant manifold. Intuitively, structures in the graph (for example, a set of vertices) that correspond to stable manifolds in the underlying dynamical system are expected to be characterized by high stretching. Therefore, to detect the structures of interest, we calculate a local expansion for each vertex by analyzing a small neighborhood subgraph for each vertex. Roughly speaking, if this neighborhood, which forms a small subgraph, is elongated, the vertex is likely to be a part of or at least close to a stable manifold. We measure this stretching by a set of different expansion values of the subgraph like e.g. (i) the number or weights of vertices in the subgraph or (ii) the number or sum of weights of the edges connecting the subgraph with the rest of the graph.

As before (see Section 3.3), let $G = (V, E)$ be a graph with vertex set V and edge set E, let $vw : V \to \mathbb{R}$ be a weight function on the vertices and let $ew : E \to \mathbb{R}$ be a weight function on the edges. For some $S \subset V$ let $W(S) := \sum_{v \in S} vw(v)$ and for some $F \subset E$ let $W(F) := \sum_{e \in F} ew(e)$. For some $S \subset V$ let $\overline{S} := V \setminus S$. For some $S, T \subset V$ let $E_{S,T} := \{\{u, v\} \in E; u \in S, v \in T\}$. In the following statement, different definitions for the expansion of a vertex v are given.

The basis for our calculations of expansion values for each vertex are the properties of the subgraphs induced by the neighborhood of each vertex. For each vertex we consider the set of neighboring vertices $U_d(v)$. This set is comprised of all vertices that can be reached from v by a path of maximum length d, where d is a small positive integer. As such paths can be seen as pseudo-solutions with respect to the initial value v, we expect that they exhibit similar qualitative characteristics as the respective trajectories in the underlying dynamical system. We therefore expect that the use of measures related to the size or weight of $U_d(v)$ can pinpoint areas of high stretching in the graph and, thus, in the underlying dynamical system.

Definition 1 (*Expansion of a vertex*). For a vertex $v \in V$ let $U(v) := U_d(v)$ be the set of vertices from V with a fixed distance of at most d from v. We consider the following definitions $\Lambda_{(z,d)}(v)$ for the **expansion of a vertex** v:

$$\begin{aligned} \Lambda_{(1,d)}(v) &= |U(v)| & \Lambda_{(3,d)}(v) &= W(E_{U(v),U(v)}) \\ \Lambda_{(2,d)}(v) &= W(U(v)) & \Lambda_{(4,d)}(v) &= W(E_{U(v),\overline{U(v)}}) \end{aligned} \tag{7}$$

$\Lambda_{(1,d)}(v)$ considers the number of vertices in the subgraph with the expectation that vertices in areas of high stretching typically span a large subgraph. $\Lambda_{(2,d)}(v)$ is the sum of the vertex weights of the subgraph, $\Lambda_{(3,d)}(v)$ the sum of the edge weights of edges within the subgraph, whereas $\Lambda_{(4,d)}(v)$ measures the weights of edges connecting the subgraph with the rest of the graph.

If the graph is derived from a volume-preserving dynamical system with equally sized boxes being the vertices, i.e. $V = \mathscr{B} = \{B_1, \ldots, B_n\}$ then these four definitions are very closely related. In this case, we obtain $\mu(B)\Lambda_{(1,d)}(B) = \Lambda_{(2,d)}(B)$ for all $B \in \mathscr{B}$, where μ denotes the volume measure. Moreover, large $\Lambda_{(1,d)}(B)$ result in a large sum of edge weights and hence in a high value of $\Lambda_{(3,d)}(B)$. One can also expect that from a large subgraph one can find many edges connecting to the rest of the graph and thus a large $\Lambda_{(4,d)}(B)$. Therefore, in our context, for equally sized boxes all four heuristics should give very similar results. Different box sizes can, for instance, result from an adaptive scheme and will be discussed later.

How does graph expansion relate to almost invariant sets and barriers to transport? From a dynamical systems point of view we can compare graph expansion to the direct expansion rates as described in Section 4.1. Via the results in [24] we can then relate high graph expansion to invariant manifolds and transport barriers. We now derive some estimates in order to be able to compare the two expansion concepts.

Proposition 1 (cf. [24]). *Let $\bar{x}$ be the center point of a box B, $N \in \mathbb{N}$ and $\varepsilon > 0$.* Then

$$\Lambda_\varepsilon(N, \bar{x}) \leqslant \delta_\varepsilon(N, B)$$

and

$$\lim_{B \to \bar{x}} \delta_\varepsilon(N, B) = \Lambda_\varepsilon(N, \bar{x})$$

that is when the box size goes to zero reducing to its center point.

So we can assume that for reasonably small boxes $\Lambda_\varepsilon(N, \bar{x})$ will be a good approximation to $\delta_\varepsilon(N, B)$ [24].

Lemma 1. *Let $f : \mathbb{R}^m \to \mathbb{R}^m$ and $\mathscr{B}$ be a box covering of $M \subset \mathbb{R}^m$ consisting of equally sized boxes B_i, $i = 1, \ldots, n$ with equal side lengths $2r$ (e.g. square or cubic boxes). Let $\bar{x}$ be the center point of a box B and $N \in \mathbb{N}$. Define*

$$\gamma_r(N, \bar{x}) := \max_{\{x : |\bar{x} - x| = r\}} \frac{|f^N(\bar{x}) - f^N(x)|}{r}.$$

Note that $\Lambda_r(N, \bar{x}) = \frac{1}{N} \log \gamma_r(N, \bar{x})$. Then

$$\max(1, \lfloor \gamma_r(N, \bar{x}) \rfloor) \leqslant \Lambda_{(1,N)}(B).$$

For $N = 1$ we get an upper bound by

$$\Lambda_{(1,1)}(B) \leqslant \lceil \gamma_r(1, \bar{x}) + 1 \rceil^m$$

Proof. $\gamma_r(N, \bar{x})$ gives the factor by which an inscribed ball in the box is stretched under one iteration of the map. As f is continuous the images of B will be connected, intersecting at least $C = \max(1, \lfloor \gamma_r(N, \bar{x}) \rfloor)$ boxes. So $C \leqslant |U_N(B)|$, where $U_N(B)$ is the graph of radius N induced by the vertex (box) B. For $N = 1$ the image of the ball with radius r and center $\bar{x}$ is contained in a ball of radius $r \cdot \gamma_r(N, \bar{x})$. Thus, $(\lceil \gamma_r(N, \bar{x}) \rceil + 1)^m$ is the maximum number of boxes needed to cover this ball, where m refers to the dimension of phase space. □

Lemma 1 gives coarse bounds on the graph expansion. If a box has a high expansion rate then we can conclude that it will also have a high graph expansion. Moreover, for $N = 1$ the graph expansion has an upper bound related to the box expansion. For $N > 1$ there is no such estimate on an upper bound. This is because a path in $U_N(B)$ does typically not correspond to a true trajectory of f. Nevertheless we can get an estimate of the local graph expansion for $N > 1$ by considering the expansion of the vertices contained in the subgraph.

Lemma 2. *Set $U_0(B) := B$ and $U_k(B)$, $k \in \mathbb{N}$, as defined previously. For $l = 1, \ldots, k-1$ define $X_l(B) := U_{k-l}(B) \setminus U_{k-(l+1)}(B)$. Then*

$$\Lambda_{(1,k)}(B) \leqslant \Lambda_{(1,k-1)}(B) + \sum_{\widehat{B} \in X_1 B} \Lambda_{(1,1)}(\widehat{B}) \leqslant \Lambda_{(1,1)}(B) + \sum_{l=1}^{k-1} \sum_{\widehat{B} \in X_l(B)} \Lambda_{(1,1)}(\widehat{B})$$

for $k \geqslant 2$.

Proof. Getting the new graph $U_k(B)$ from $U_{k-1}(B)$ is by adding direct neighbors to the existing graph, i.e.

$$U_k(B) = \bigcup_{\widehat{B} \in U_{k-1}(B)} U_1(\widehat{B}).$$

More strictly only the U_1 neighbors of new vertices in $U_{k-1}(B)$ have to be considered, i.e.

$$U_k(B) = U_{k-1}(B) \cup \bigcup_{\widehat{B} \in X_1(B)} U_1(\widehat{B})$$

where $X_1(B) = U_{k-1}(B) \setminus U_{k-2}(B)$.

Hence, with $\Lambda_{(1,k)}(B) = |U_k(B)|$ we obtain

$$\Lambda_{(1,k)}(B) \leqslant \Lambda_{(1,k-1)}(B) + \sum_{\widehat{B} \in X_1(B)} \Lambda_{(1,1)}(\widehat{B}).$$

So we obtain

$$\Lambda_{(1,k)}(B) \leqslant \Lambda_{(1,1)}(B) + \sum_{l=1}^{k-1} \sum_{\widehat{B} \in X_l(B)} \Lambda_{(1,1)}(\widehat{B})$$

by iteration. □

These estimates are summarized in the following

Theorem 1. *Let $k \in \mathbb{N}$, $X_l := U_{k-l}(B) \setminus U_{k-(l+1)}(B)$ for $l = 1, \ldots, k-1$, and denote by $\widehat{X}_l$ the collection of center points of X_l. Then*

$$\max(1, \lfloor \gamma_r(N, \bar{x}) \rfloor) \leqslant \Lambda_{(1,N)}(B) \leqslant (\lceil \gamma_r(1, \bar{x}) \rceil + 1)^m + \sum_{l=1}^{k-1} \sum_{\hat{x} \in \widehat{X}_l} (\lceil \gamma_r(1, \hat{x}) \rceil + 1)^m$$

The proof follows immediately from Lemmas 1 and 2. Theorem 1 relates graph expansion (i.e. the first version) to expansion rates. In particular, the box valued concept may provide a lower bound for the graph based one. The upper bound contains local expansion information about the boxes contained in $U_N(B)$. Both bounds are of course very pessimistic, but are meant to show that regions of high graph expansion are candidates for regions of high (box) expansion rates for which theoretical results with respect to invariant manifolds and transport barriers are available [24].

In the example Sections 5 and 6 we will compare expansion rates and graph expansion numerically and also consider the results of graph partitioning algorithms. Note that for all experiments we will consider the undirected graph $\overline{G} = (\mathscr{B}, \overline{E})$ with vertex weights $\mu(B_i)$ (i.e. normalized volume of box B_i) and edge weights as defined in Eq. (4). This allows us to obtain the boundaries formed by both stable and unstable manifolds simultaneously.

4.3. Adaptive graph-expansion approach

As the set-oriented discretization scheme exhibits a multilevel structure, we shortly describe a heuristic adaptive graph-expansion approach that allows us to obtain finer details of the transport barriers while keeping the computational costs at an acceptable level.

Let $\mathscr{B}$ be the box covering of M consisting of n boxes B_i, $i = 1, \ldots, n$. Denote by D the depth of the box covering, i.e. the number of subdivision steps to obtain $\mathscr{B}$.

For the given box covering we compute the associated transition matrix $P_{\mathscr{B}}$ and an approximation to the natural invariant measure μ, which in the examples considered here will correspond to the normalized box volumes. Based on this we can form the undirected graph $\overline{G} = (\mathscr{B}, \overline{E})$ with vertex weights $\mu(B_i)$ and edge weights as defined in Eq. (4). For a given heuristic $z = 1, \ldots, 4$ and a given distance d we can compute the graph expansion $\Lambda_{(z,d)}(B_i)$ for each $B_i \in \mathscr{B}$, $i = 1, \ldots, n$. In the next step we subdivide those boxes which expansion exceeds a certain value *val*, here we use $val = \frac{1}{|\mathscr{B}|}\sum_{B\in\mathscr{B}} \Lambda_{(z,d)}(B)$, i.e. the average graph expansion.

These ideas are summarized in the following algorithm:

Algorithm 1.

Initialize $\mathscr{B} = \{B_1, \ldots, B_n\}$, steps, z, d and $\Lambda_{(z,d)}(B_i)$, $i = 1, \ldots, n$.
For $k = 1 \ldots$ steps
  compute $val = \frac{1}{n}\sum_{i=1}^{n} \Lambda_{(z,d)}(B_i)$
  subdivide all boxes B_i with $\Lambda_{(z,d)}(B_i) > val$, $i = 1, \ldots, n$
  obtain $\mathscr{B}_{new}$ consisting of n_{new} boxes
  $\mathscr{B} := \mathscr{B}_{new}$, $n := n_{new}$
  compute $P_{\mathscr{B}}$, μ
  form $\overline{G} = (\mathscr{B}, \overline{E})$
  $d = d + 1$
  compute $\Lambda_{(z,d)}(B_i)$ for all $i = 1, \ldots, n$
end

This approach refines the box covering in regions of high expansion and it is thus expected to provide in each step an increasingly detailed approximation of the dominant transport barriers. By increasing the radius d by 1 after each subdivision step larger parts of the graph can be reached, ensuring robust results.

5. The Double Gyre flow

5.1. The model

We consider the periodically forced system of differential equations [6]

$$\begin{aligned} \dot{x} &= -\pi A \sin(\pi f(x,t)) \cos(\pi y), \\ \dot{y} &= \pi A \cos(\pi f(x,t)) \sin(\pi y) \frac{df}{dx}(x,t), \end{aligned} \tag{8}$$

where $f(x,t) = \epsilon \sin(\omega t)x^2 + (1 - 2\epsilon \sin(\omega t))x$, $(x,y) \in M = [0,2] \times [0,1]$, $\epsilon \geqslant 0$. Note that the boundary of M is invariant.

We fix parameter values $A = 0.25$, $\epsilon = 0.25$ and $\omega = 2\pi$ and obtain a flow of period $T = 1$. Furthermore, we fix the initial time $t_0 = 0$ and consider the time-1 flow map $f : M \to M$. f corresponds to a global Poincaré map of the periodically forced system and preserves area and orientation. The Poincaré map f possesses six hyperbolic fixed points, four of which can be found in the corners of M, with invariant manifolds located in the boundaries of M. Two other fixed points are located at $x^1_{(0)} \approx (1.08, 0)$ and $x^2_{(0)} \approx (0.92, 1)$. These nontrivial hyperbolic fixed points and the heteroclinic tangle formed by their invariant manifolds gives rise complicated dynamics: one obtains a mixed phase space structure exhibiting a chaotic sea and families of tori as shown in Fig. 1(a).

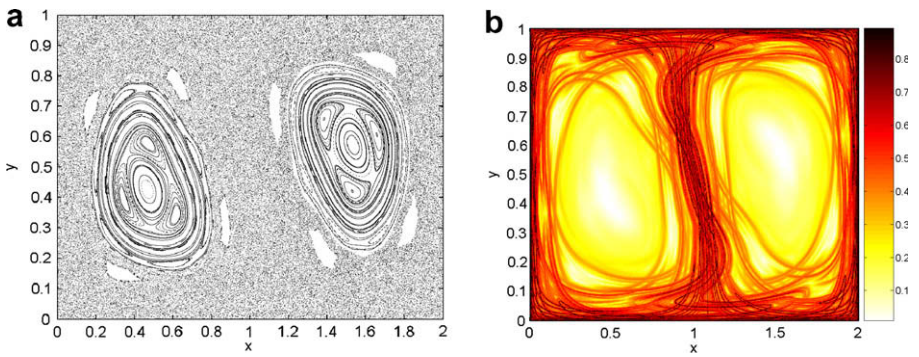

Fig. 1. Poincaré map of the Double Gyre flow. (a) Mixed phase space structure exhibiting regular and chaotic regions. (b) Expansion rate approach highlights the heteroclinic tangle and thus the major transport barriers. Dark regions correspond to high stretching whereas light regions highlight nearly no expansion in this area.

5.2. Results

The set-oriented approach as described in Section 3 is used for the numerical approximations. First we compute the expansion rate field (see Section 4.1). For this we use a box covering of M on depth $D = 18$, consisting of $n = 262,144$ equally sized boxes. We choose $N = 10$, $\varepsilon = 4 \times 10^{-4}$ and compute $\delta_\varepsilon(N, B)$ for all boxes B using 20 pairs of test points in each box. In addition we compute the expansion rate field $\bar{\delta}_\varepsilon(N, B)$ for the time-reversed system. In fact, regions of high values in $\delta_\varepsilon(N, \cdot)$ are found to be in the vicinity of the stable manifold of $x^1_{(0)}$, $\bar{\delta}_\varepsilon(N, \cdot)$ highlights the unstable manifold of $x^2_{(0)}$. Fig. 1(b) shows both fields via $\max(\bar{\delta}_\varepsilon(N, B), \delta_\varepsilon(N, B))$. Note that the major transport barrier is formed by a heteroclinic connection of these manifolds and divides M into two halves.

For the graph based investigation we start with a box covering of the rectangle $M = [0, 2] \times [0, 1]$ on depth $D = 14$ with 16,384 boxes. For the computation of the transition matrix $P_{\mathscr{B}}$ (see Eq. (2)) we employ a uniform inner grid of 10×10 points in each box. We compute μ (here normalized box volumes) and form the undirected graph $\overline{G}$ as described previously.

Fig. 2 shows a decomposition of our relevant region into five and 10 sets. The partition into five sets matches very well the decomposition into regular and chaotic regions as visible in Fig. 1(a) but misses the transport barrier built by the invariant manifolds.

The decomposition into 10 sets discloses more structure in the regular regions but also picks up the relevant transport barrier related to the invariant manifolds. So using the graph partitioning approach we are able to detect the important structures of the underlying system without using any geometric information of the dynamics. In this specific partition we have an average internal cost of approximately 0.97 (see Eq. (5)). That means that on average 97% of the particles initialized in one of the sets will stay in the respective set after one iteration of the map f.

While as demonstrated above the graph partitioning technique finds the dynamically interesting transport barriers only after decomposition into at least 10 sets, the graph based expansion finds this boundary immediately, see Fig. 3. For the computation of the graph based expansion we used the four heuristics described in Definition 7. In accordance with the observations when applying expansion rate approach (see [24]), also in graph expansion one obtains the more structure the longer the distance d is chosen. As expected all methods give very similar results. Because the values of $\Lambda_{(1,d)}$ and $\Lambda_{(2,d)}$ are equal up to a constant factor, we only show $\Lambda_{(2,d)}$.

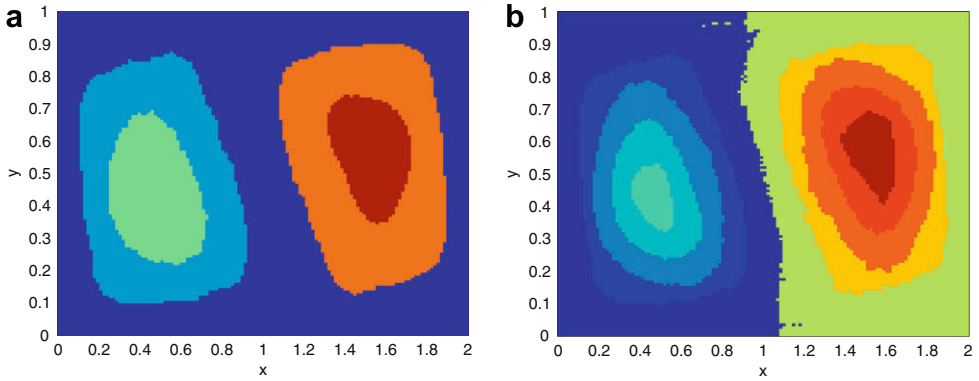

Fig. 2. Partition of the phase space into five (a) and 10 sets (b) using one of the graph partitioning heuristics implemented in PARTY [31].

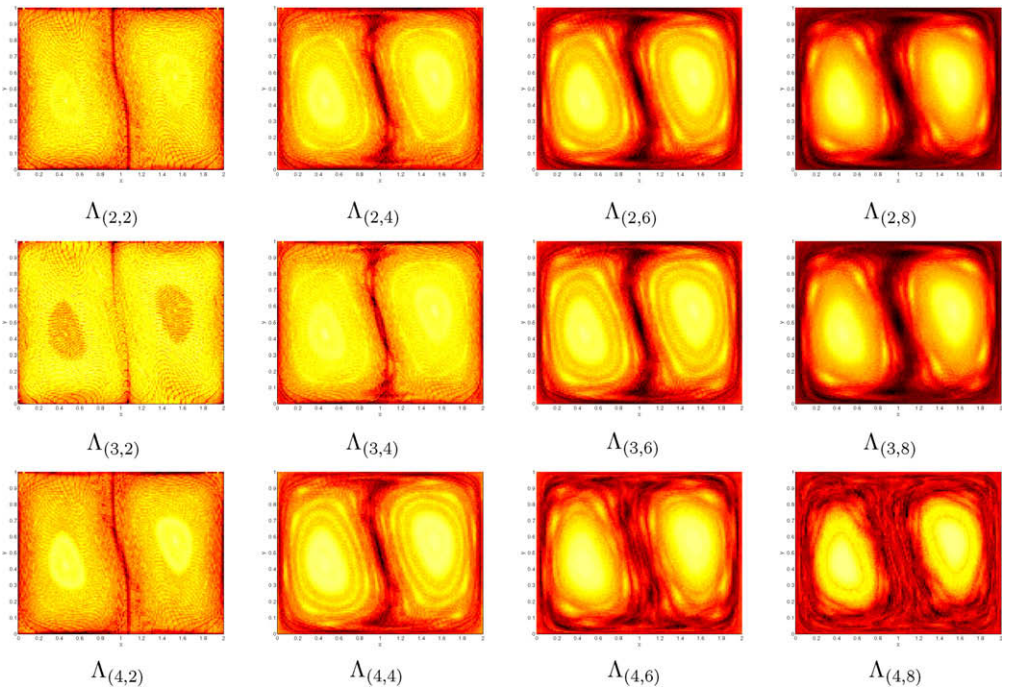

Fig. 3. Graph based expansion for the Double Gyre with respect to a box covering on depth $D = 14$ (16,384 boxes). The results for the different heuristics $\Lambda_{(z,d)}$ for $z = 2, 3, 4$ and $d = 2, 4, 6, 8$ are shown. Dark colors correspond to areas of high stretching and indicate the location of transport barriers. The heteroclinic tangle formed by the invariant manifolds of the hyperbolic fixed points is clearly visible.

Again, dark colors indicate regions of high expansion whereas light colors correspond to low expansion (i.e. regular behavior). The heteroclinic tangle formed by the invariant manifolds of the hyperbolic fixed points can be well seen in all plots and compares well to the expansion rate results in Fig. 1, especially for large diameters d.

Already this simple example illustrates that the graph formulation retains the relevant dynamical information of the underlying system. Moreover, graph expansion appears to compare very well to the expansion rate approach and is thus able to pinpoint the major transport barriers.

5.3. Adaptive approach

The adaptive approach introduced in Section 4.3 allows for highlighting the relevant transport barriers even more clearly. We start with a box covering of M on depth $D = 10$ with 1024 boxes and fix $z = 1$, $d = 2$ and *steps* $= 8$. The graph expansion values for the initial box collection are shown in Fig. 4(a), with the colors chosen as before. The result after four steps of the algorithm is demonstrated in Fig. 4(b). Here the heteroclinic tangle is nicely highlighted and compares well to the respective results in Fig. 3 ($d = 6$). Note that for the adaptive covering only 5504 boxes are needed compared to 16,384 for a regular discretization. The graph expansion for the respective adaptive covering after eight steps is plotted in Fig. 4(c). Here we obtain a very clear transport barrier that directly relates to the relevant heteroclinic connection. The covering contains only 38,152 boxes whereas a regular discretization on depth $D = 18$ consists of 262,144 boxes.

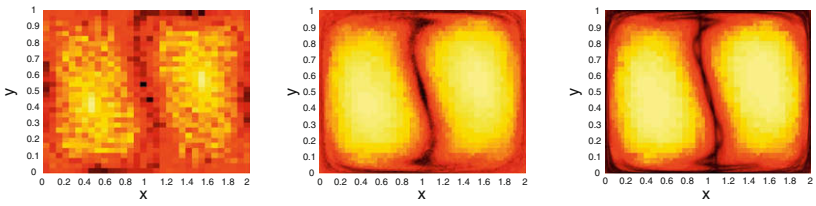

(a) $\Lambda_{(1,2)}, D = (10, 10)$ (b) $\Lambda_{(1,6)}, D = (10, 14)$ (c) $\Lambda_{(1,10)}, D = (10, 18)$

Fig. 4. Adaptive graph based expansion for the Double Gyre starting with a box covering on depth $D = 10$. The results for the first heuristic $\Lambda_{(1,d)}$ are shown. Dark colors indicate high graph expansion.

6. The Planar Circular Restricted Three Body Problem

6.1. The model

We consider the planar circular restricted three body problem (PCR3BP) with the Sun and Jupiter as main bodies, with masses m_1 and m_2, respectively. The mass m_3 of the third body – typically an asteroid, a comet, a spacecraft or just a particle – is assumed to be negligible. The PCR3BP is a particular case of the general gravitational problem of the three masses $m_1,\ m_2,\ m_3$. The motion of all three bodies takes place in a common plane where the masses m_1 and m_2 move on circular orbits about their common center of mass. Since the third body has zero mass it does not influence the motion of the main bodies. Normalizing the total mass we obtain a nondimensional representation of the two masses as $1-\epsilon$ (Sun) and ϵ (Jupiter), where $\epsilon = m_2/(m_1+m_2)$. In our considered case that means $\epsilon = 9.5368\times 10^{-4}$. For a detailed derivation of the equations of motion we refer to [39] and restrict ourselves to the basics.

Choosing a rotating coordinate system so that the origin is at the center of mass, the Sun and Jupiter are on the x-axis at the points $(-\epsilon,0)$ and $(1-\epsilon,0)$, respectively. (x,y) will denote the position of the particle in the plane, then the equations of motion for the particle in this rotating frame are given by

$$\ddot{x}-2\dot{y}=\Omega_x,\quad \ddot{y}+2\dot{x}=\Omega_y, \tag{9}$$

where

$$\Omega=\frac{x^2+y^2}{2}+\frac{1-\epsilon}{r_1}+\frac{\epsilon}{r_2}+\frac{\epsilon(1-\epsilon)}{2}.$$

Here, the subscripts of Ω denote partial differentiation in the respective variable, and $r_1,\ r_2$ are the distances from the particle to the Sun and Jupiter, respectively.

Using a Legendre transformation the autonomous equations (9) can be put into Hamiltonian form. The system has a first integral – the Jacobi integral – which is given by

$$C(x,y,\dot{x},\dot{y})=-(\dot{x}^2+\dot{y}^2)+2\Omega(x,y).$$

C is also called the Jacobi constant.

Hence, the motion of the test particle takes place on a three-dimensional energy manifold (defined by a particular value of C) embedded in the four-dimensional phase space, $(x,y,\dot{x},\dot{y})$. The value of the Jacobi constant is an indicator of the type of global dynamics possible for a particle in the PCR3BP, see [40] for a discussion. We will focus on the case shown in Fig. 5(a) and consider for all the following computations in this section a Jacobi constant given by $C=3.05$. Here the particle is trapped either exterior or interior to the planet's orbit, or in the region around the planet.

Furthermore, we consider the Poincaré surface-of-section (s-o-s) defined by $y=0,\ \dot{y}>0$. The coordinates of that section are $(x,\dot{x})$ – that means, we plot the x coordinate and the velocity of the test particle at every conjunction with the planet. Also, we restrict ourselves to the motion of the test particles in the exterior region. For orbits exterior to the planet's, the s-o-s is crossed every time the test particle is aligned with the Sun and Jupiter and is on the opposite side of the Sun from the planet. Thus, the s-o-s becomes the two-dimensional manifold M defined by

$$y=0,\quad \dot{y}>0,\quad x<-1, \tag{10}$$

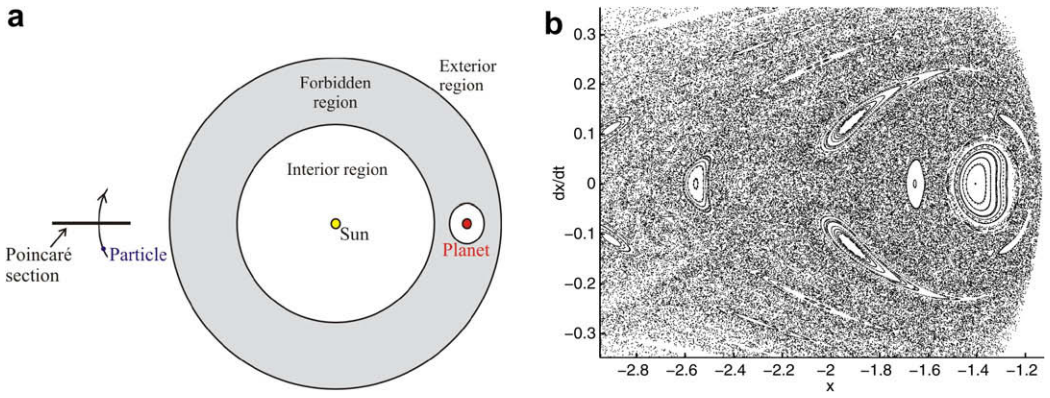

Fig. 5. (a) The Sun and planet are fixed in this rotating frame. Here, the particle is trapped either exterior or interior to Jupiter's orbit, or around Jupiter itself. It is energetically prohibited from crossing the *forbidden region,* shown in gray. As the energy E of the particle increases, the bottlenecks connecting the regions open and, finally, the entire configuration space is energetically accessible. (b) The mixed phase space structure of the PCR3BP, exhibiting regular and chaotic regions is shown on this s-o-s.

reducing the system to an area and orientation preserving map $f : M \to M$ on a subset M of $\mathbb{R}^2$. Fig. 5(a) illustrates our choice of the Poincare surface-of-section. Taking a sample of initial conditions on this s-o-s and following their images under repeated iteration of the return map, gives a good indication of the mixed phase space structure consisting of regular regions (e.g. KAM tori) embedded within a "chaotic sea" (see Fig. 5(b)). There is a hyperbolic fixed point approximately given by $(\bar{x}, \dot{\bar{x}}) \approx (-2.0295796, 0)$, whose stable and unstable manifolds form a major barrier to the transport of asteroids [7]. However, similar to the previous example, direct integration as in Fig. 5(b) cannot reveal these transport barriers within the chaotic sea. In order to detect these structures directly we will again employ the local expansion rate approaches.

6.2. Results

For the Poincaré map $f : M \to M$ we consider M to be the chain recurrent set within the rectangle $X = [-2.95, -1.05] \times [-0.45, 0.55]$ in the section $y = 0,\ \dot{y} > 0,\ x < -1$. M is covered by a collection of 137,840 equally sized boxes on depth $D = 18$.

Choosing $N = 3$ iterations of f the set-oriented expansion rate field in forward and backward time is computed and plotted using the same set-up as in the previous example of the Double Gyre.

This approach detects the major transport barriers corresponding to stable and unstable manifolds of the hyperbolic fixed point $(\bar{x}, \dot{\bar{x}})$ of f. Moreover, the expansion rate approach highlights the complicated homoclinic tangles that provide the basis for the transport mechanism (see Fig. 6(a)). Regions with low expansion are predominantly regular regions (tori) shown in light color. Dark colored regions correspond to high expanding areas. In order to be able to compare the expansion rate results with the graph based concepts we numerically extract the major transport barriers for this example (see Fig. 6(b)).

To illustrate that these structures serve as transport barriers we follow a sample of points initialized in different almost invariant sets under repeated iteration of the map f, see Fig. 6(c) and (d). We use initial conditions from two different sets, depicted by the 400 black and 250 white dots (·). These points are mapped for one (Fig. 6(c)) and for five (Fig. 6(d)) iterations, where the black diamonds (◇) and white circles (○) mark the respective end points. As expected from the notion of almost invariance there is hardly any transport between the two regions – even after five iterations.

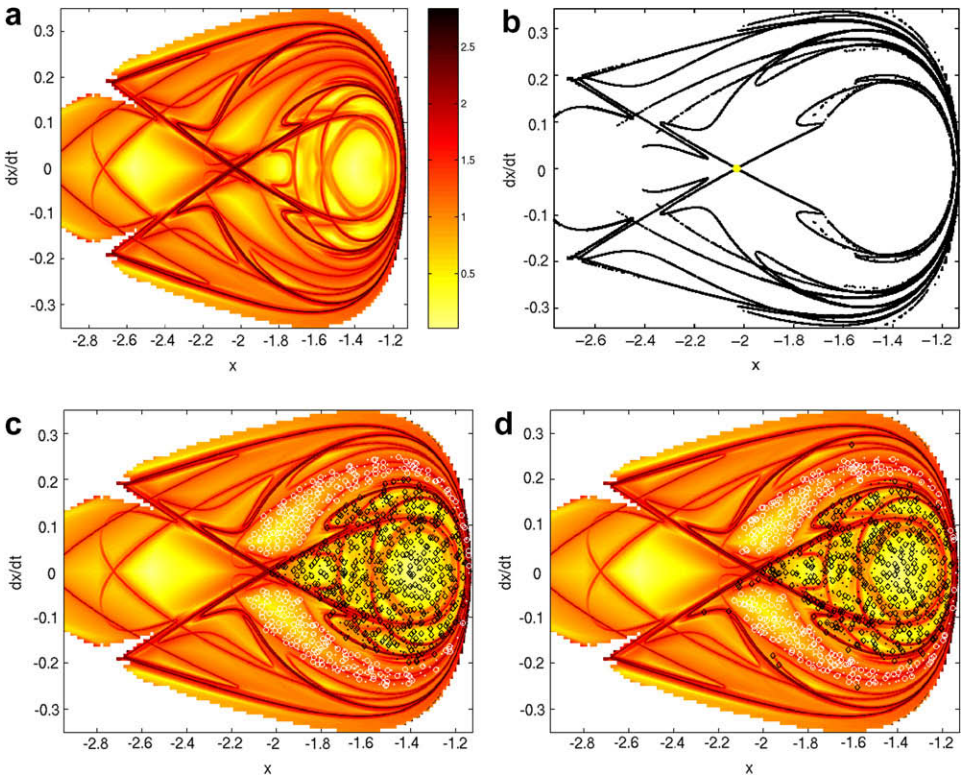

Fig. 6. (a) Approximation of transport barriers (here, the stable and unstable manifold of a hyperbolic fixed point) using a set-oriented expansion rate approach. Dark areas correspond to high stretching, computed using three iterations of f in forward and backward time. The relevant region in phase space is covered by a collection of small boxes. (b) Extraction of relevant barriers. (c + d) Direct integration of a sample of initial conditions in two different almost invariant sets (marked by black and white dots (·)). White ○ and black ◇ mark the end points after one (c) and five (d) iterations of the map f. As expected, nearly all sample points remain in their initial set such that there is hardly any transport between the two sets.

Returning to the graph based concepts, we again use a uniform innergrid of 10×10 points for the computation of the transition matrix $P_{\mathscr{B}}$. Dominant almost invariant regions in the Sun–Jupiter problem approximated via graph partitioning techniques are shown in Fig. 7. The internal cost of this specific decomposition into seven sets is approximately 0.98. Fig. 7(b) illustrates there is a very good agreement between part of the decomposition and the boundary extracted using the expansion rate approach. So again the geometric information related to invariant manifolds and high expansion rates appears to be well coded in the graph. Nevertheless, as in the previous example the graph partitioning approach first restricts to decomposing M into regular and chaotic regions. Only when allowing a relatively high number of sets, a decomposition related to the invariant manifolds of the hyperbolic fixed point of f is obtained – and thus the dynamically relevant transport barriers we are interested in.

Fig. 8 shows computations of the graph based expansion approach for two different heuristics $z = 2$ and $z = 4$. Again, the computation diameter varies between $d = 2,\ 4,\ 6$ and $d = 8$, and we colored each box (i.e. each vertex v) according to the expansion value of the respective neighborhood subgraph of radius d induced by v.

In this example, traces of the relevant transport barriers are already visible for a small choice of d. For larger values of the radius d the approximated structures match increasingly better with transport barriers obtained via the expansion rate approach described above.

7. Conclusion and future directions

As demonstrated above the combination of geometrical and graph based methods provides a powerful tool for the qualitative and quantitative analysis of transport in dynamical systems. Both the set-oriented expansion rate approach and the graph partitioning ansatz define consistent almost invariant regions. This is in good agreement with related work on almost

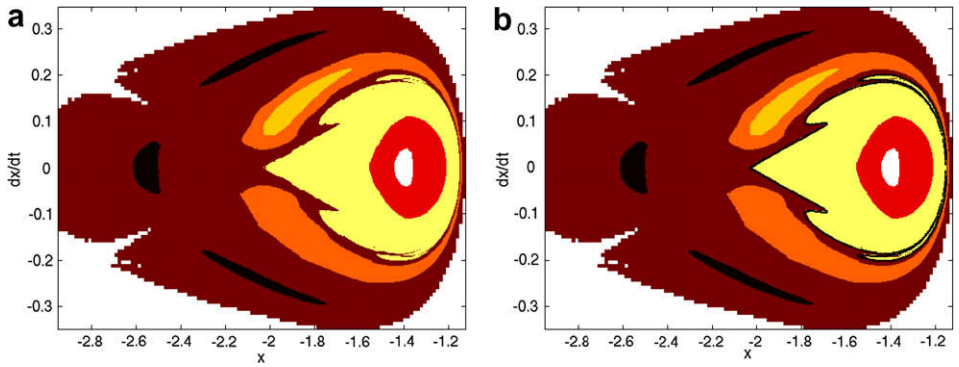

Fig. 7. Partition of the chain recurrent set into seven sets (a) without and (b) with parts of the boundary. The boundary is extracted using the results from the expansion rate approach.

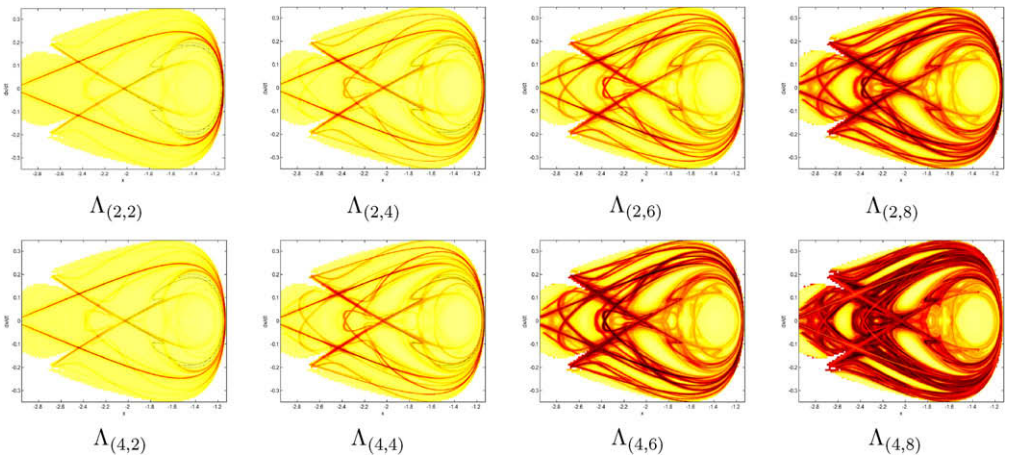

Fig. 8. Graph based expansion for the PCR3BP with respect to a box covering of the chain recurrent set on depth 18 (137,840 boxes). The results for the different heuristics $\Lambda_{(z,d)}$ for $z = 2,\ 4$ and $d = 2,\ 4,\ 6,\ 8$ are shown. Here vertices that induce particularly expansive subgraphs are highlighted by dark colors. The results compare very well to the expansion rate approach.

invariant sets and invariant manifolds [12]. The application of graph based expansion compares well to the expansion rate approach and confirms that the reduction of the dynamical system f to a discrete graph with a finite-state Markov process retains all relevant information from the dynamics. Like the expansion rate approach graph based expansion reliably finds the dynamically relevant transport barriers whereas graph partitioning first restricts to decomposing phase space into regular and chaotic regions.

In the astrodynamical application considered here, the results allow us to draw conclusions about transport of particles between the Jupiter region and a neighborhood of the Sun. In particular, based on the approximation of the relevant sets we can now compute transition probabilities and estimate for instance the risk of an asteroid impact, as discussed in Dellnitz et al. [7,23].

Future research will be include the improvement of the so far very coarse analytical results as well as a comparison of graph expansion to the notion of graph congestion [22]. Moreover, the graph based expansion ansatz is computationally inexpensive compared to partitioning methods and it can probably be used to obtain an initial guess for the solution of graph partitioning problems. In particular, for the analysis of dynamical systems graph based expansion appears to find the relevant boundaries more reliably than graph partition. So a combination of these concepts will potentially improve the quality of the resulting decomposition into almost invariant sets. In a more general context, graph expansion may also be applied to define and find analogue structures to hyperbolic fixed points in graphs. Finally, future work may also include the detection of other transport barriers such as cantori.

Acknowledgements

This research was partly supported by the EU funded Marie Curie Research Training Network *AstroNet*. K.P. is grateful for partial support by the Gottlieb Daimler- und Karl Benz Stiftung.

References

[1] Wiggins S. Chaotic transport in dynamical systems. New York (NY): Springer; 1992.
[2] MacKay R, Meiss J, Percival I. Transport in Hamiltonian systems. Physica D 1984;13:55–81.
[3] Rom-Kedar V, Wiggins S. Transport in two-dimensional maps. Arch Ration Mech Anal 1990;109:239–98.
[4] Haller G. Finding finite-time invariant manifolds in two-dimensional velocity fields. Chaos 2000;10:99–108.
[5] Meiss J. Symplectic maps, variational principles, and transport. Rev Mod Phys 1992;64(3):795–848.
[6] Shadden S, Lekien F, Marsden J. Definition and properties of Lagrangian coherent structures from finite-time Lyapunov exponents in two-dimensional aperiodic flows. Physica D 2005;212:271–304.
[7] Dellnitz M, Junge O, Koon W, Lekien F, Lo M, Marsden J, et al. Transport in dynamical astronomy and multibody problems. Int J Bifurcat Chaos 2005;15(3):699–727.
[8] Broer H, Hanßmann H. Hamiltonian perturbation theory (and transition to chaos). In: Meyers R, editor. Encyclopaedia of complexity & system science. Springer, in press.
[9] Aref H. The development of chaotic advection. Phys Fluids 2002;14(4):1315–25.
[10] Wiggins S. The dynamical systems approach to Lagrangian transport in oceanic flows. Annu Rev Fluid Mech 2005;37:295–328.
[11] Gladman B, Burns J, Duncan M, Lee P, Levison H. The exchange of impact ejecta between terrestrial planets. Sciences 1996;271:1387–92.
[12] Froyland G, Padberg K. Almost-invariant sets and invariant manifolds – connecting probabilistic and geometric descriptions of coherent structures in flows. Physica D 2009 (in press).
[13] Haller G. Distinguished material surfaces and coherent structures in three-dimensional fluid flows. Physica D 2001;149:248–77.
[14] Haller G, Poje A. Finite-time transport in aperiodic flows. Physica D 1998;119:352–80.
[15] Haller G, Yuan G. Lagrangian coherent structures and mixing in two-dimensional turbulence. Physica D 2000;147:352–70.
[16] Dellnitz M, Junge O. On the approximation of complicated dynamical behavior. SIAM J Numer Anal 1999;36(2):491–515.
[17] Deuflhard P, Dellnitz M, Junge O, Schütte C. Computation of essential molecular dynamics by subdivision techniques. In: Deuflhard P et al. editor. Computational molecular dynamics: challenges, methods, ideas, LNCSE, vol. 4. Springer-Verlag; 1998. p. 98–115.
[18] Deuflhard P, Huisinga W, Fischer A, Schütte C. Identification of almost invariant aggregates in reversible nearly uncoupled Markov chains. Lin Alg Appl 2000;315:39–59.
[19] Huisinga W. Metastability of Markovian systems, Ph.D. thesis, Freie Universität Berlin; 2001.
[20] Froyland G, Dellnitz M. Detecting and locating near-optimal almost-invariant sets and cycles. SIAM J Sci Comput 2003;24:1839–63.
[21] Deuflhard P, Weber M. Robust Perron cluster analysis in conformation dynamics. Linear Algebra Appl 2005;398:161–84.
[22] Dellnitz M, Preis R. Congestion and almost invariant sets in dynamical systems. In: Winkler F, editor. Proceedings of SNSC'01, Springer; 2003. p. 183–209.
[23] Dellnitz M, Junge O, Lo MW, Marsden JE, Padberg K, Preis R, et al. Transport of Mars-crossers from the quasi-Hilda region. Phys Rev Lett 2005;94(231102):1–4.
[24] Padberg K. Numerical analysis of transport in dynamical systems, Ph.D. thesis, Universität Paderborn, Germany, June; 2005.
[25] Dellnitz M, Hohmann A. A subdivision algorithm for the computation of unstable manifolds and global attractors. Numer Math 1997;75:293–317.
[26] Dellnitz M, Froyland G, Junge O. The algorithms behind GAIO – set oriented numerical methods for dynamical systems. In: Fiedler B, editor. Ergodic theory, analysis, and efficient simulation of dynamical systems. Springer; 2001. p. 145–74.
[27] Ulam S. A collection of mathematical problems. Interscience Publishers; 1960.
[28] Hunt F. A Monte Carlo approach to the approximation of invariant measures. Random Comput Dyn 1994;2:111–33.
[29] Froyland G. Statistically optimal almost-invariant sets. Physica D 2005;200:205–19.
[30] Garey M, Johnson D. Computers and intractability – a guide to the theory of NP-completeness. Freeman; 1979.
[31] Preis R. Analyses and design of efficient graph partitioning methods, Ph.D. thesis, Universität Paderborn, Germany, November; 2000.
[32] Hendrickson B, Leland R. A multilevel algorithm for partitioning graphs. In: Supercomputing'95: proceedings of the 1995 ACM/IEEE conference on supercomputing (CDROM). New York, NY, USA: ACM; 1995. p. 28.
[33] Walshaw C. The Jostle user manual: version 2.2, University of Greenwich; 2000.
[34] Karypis G, Kumar V. A fast and high quality multilevel scheme for partitioning irregular graphs. SIAM J Sci Comput 1998;20(1):359–92.
[35] Pellegrini F. SCOTCH 3.1 user's guide, Tech. Rep. 1137-96, LaBRI, University of Bordeaux; 1996.
[36] Monien B, Preis R, Diekmann R. Quality matching and local improvement for multilevel graph-partitioning. Parallel Comput 2000;26(12):1609–34.
[37] Preis R. GADS – graph algorithms for dynamical systems, Tech. Rep., Universität Paderborn; 2004.

[38] Dellnitz M, Padberg K, Preis R. Integrating multilevel graph partitioning with hierarchical set oriented methods for the analysis of dynamical systems, Tech. Rep., Preprint 152, DFG priority program: analysis, modeling and simulation of multiscale problems; 2004.
[39] Szebehely V. Theory of orbits. Academic Press; 1967.
[40] Koon W, Lo M, Marsden J, Ross S. Heteroclinic connections between periodic orbits and resonance transitions in celestial mechanics. Chaos 2000;10(2):427–69.